HHS Public Access

Author manuscript

Nat Neurosci. Author manuscript; available in PMC 2014 April 01.

Published in final edited form as:

Nat Neurosci. 2013 October ; 16(10): 1461–1467. doi:10.1038/nn.3511.

Neuropeptide signaling remodels chemosensory circuit composition in *Caenorhabditis elegans*

Sarah G. Leinwand[1,2] and **Sreekanth H. Chalasani**[1,2,3]

[1]Neurosciences Graduate Program, University of California, San Diego, La Jolla, CA 92093

[2]Molecular Neurobiology Laboratory, The Salk Institute for Biological Studies, La Jolla, CA 92037

Abstract

Neural circuits detect environmental changes and drive behavior. The routes of information flow through dense neural networks are dynamic; however, the mechanisms underlying this circuit flexibility are poorly understood. Here, we define a novel, sensory context-dependent and neuropeptide-regulated switch in the composition of a *C. elegans* salt sensory circuit. The primary salt detectors, ASE sensory neurons, use BLI-4 endoprotease-dependent cleavage to release the insulin-like peptide INS-6 in response to large but not small changes in external salt stimuli. Insulins, signaling through the insulin receptor DAF-2, functionally switch the AWC olfactory sensory neuron into an interneuron in the salt circuit. Animals with disrupted insulin signaling have deficits in salt attraction, suggesting that peptidergic signaling potentiates responses to high salt stimuli, which may promote ion homeostasis. Our results show that sensory context and neuropeptide signaling modify neural networks and suggest general mechanisms for generating flexible behavioral outputs by modulating neural circuit composition.

All sensory circuits use specialized sensory neurons to detect environmental changes and downstream interneurons to transform that information, generating flexible behaviors. In particular, chemosensory neural circuits have an additional challenge of representing not only commonly encountered cues, but also a potentially limitless set of novel smell and taste stimuli[1]. One approach to understanding how chemical cues drive behavior is to trace the paths of information flow in the corresponding neural circuits. This task is difficult because the active route through networks of anatomically connected sensory, inter- and motor neurons can also switch based on context, as observed in circuits processing nutrients[2] and light[3]. Therefore, the underlying molecular mechanisms that configure active neural circuits are poorly understood. The *C. elegans* nervous system, with just 302 neurons connected by identified synapses[4], is ideally suited for a circuit-level analysis of how chemosensory stimuli are represented and transformed into behavioral outputs[5].

[3]Author for correspondence: schalasani@salk.edu.

AUTHOR CONTRIBUTIONS

S.G.L. conceived and conducted the experiments, interpreted the data and co-wrote the paper. S.H.C. conceived the experiments, interpreted the data and co-wrote the paper.

Cell ablation experiments in *C. elegans* identified individual sensory neurons critical for directed locomotion towards chemical stimuli. In particular, the ASE sensory neurons are necessary to drive attraction to salts, while the AWC sensory neurons drive attraction to odors (Supplementary Fig. 1a)[6]. The neural circuitry acting downstream of these neurons to drive behavior has not been fully mapped; however, neuroanatomical studies identify a set of common interneuron targets, including AIA (Fig. 1a)[4]. Interestingly, the pair of bilateral ASE neurons are functionally distinct: ASELeft (ASEL) detects an increase in sodium chloride (NaCl) and ASERight (ASER) responds to a decrease in NaCl[7]. Similarly, the two AWC neurons, AWC^{ON} and AWC^{OFF}, collectively respond to the odorant benzaldehyde and uniquely respond to other odorants[8]. Here, we combine genetic manipulations, *in vivo* calcium imaging and behavioral analysis to investigate how the functional ASE-driven salt circuit represents specific changes in salt to drive dynamic behavioral responses. *C. elegans*, much like mammals, prefer a concentration of salt that maintains ion homeostasis, providing a physiological correlate for salt attraction behavior[9, 10]. We find that insulin neuropeptide signaling transiently remodels the composition of the salt neural circuit and modulates behavior in response to high, but not low, salt stimuli by switching the AWC^{ON} olfactory sensory neuron into an interneuron.

RESULTS

A distributed neural network encodes salt concentration

To characterize the functional neural circuit representing salt stimuli, we recorded neural activity from the anteriorly localized amphid sensory neurons using genetically expressed calcium indicators of the GCaMP family. Calcium signals in *C. elegans* neurons have been shown to strongly correlate with neuronal depolarization[11, 12]. Previous studies have shown that ASEL neurons are activated by the addition of NaCl stimuli greater than or equal to 10 mM[7] (Fig. 1b, Supplementary Figs. 1b and 2a), while ASER is sensitive to removal of at least 1 mM NaCl[7] (Supplementary Fig. 2c, e). Unexpectedly, we found that AWC^{ON} olfactory sensory neurons respond to a +50 mM increase in NaCl, much like ASEL (Fig. 1b, Supplementary Figs. 1b and 2b, Supplementary Movie 1). AWC^{OFF} neurons respond similarly to +50 mM NaCl (Supplementary Fig. 2d). In contrast, a weaker +10 mM increase in NaCl only activates ASEL, but not AWC^{ON} (Fig. 1c, Supplementary Figs. 1c and 2b), or AWC^{OFF} (Supplementary Fig. 2f). AWC^{ON} responses to salt are dose-dependent and have a threshold of +20 mM NaCl (Supplementary Fig. 2b). Furthermore, AWC^{ON} specifically responds to salt and is not a generalized osmolarity sensor (Supplementary Fig. 2g). Moreover, there is specificity in the salt circuit as other amphid sensory neurons AWA, ASI, ASK, AWB and ASH do not respond to increases in NaCl (Fig. 1b, Supplementary Fig. 2h). These results show that the *increase* in salt concentration is not encoded by the specialized responses of unimodal neurons, as was predicted from earlier cell ablation studies[6]. Instead, the combined activity of multiple sensory neurons represents external salt concentrations: ASEL together with polymodal AWC^{ON} encode larger than 20 mM increases in salt. Finally, these experiments complement studies showing that a distinct, but similarly distributed circuit encodes the *decrease* in salt concentration[13].

AWC neurons play key role in the salt circuit and behavior

We further investigated the role of AWC sensory neurons in the salt circuit by recording activity from a downstream interneuron, AIA, which receives inputs from both AWC and ASE neurons[4] (Fig. 1a). AIA interneurons respond to an increase of +50 mM NaCl (Fig. 1d, Supplementary Fig. 1d). These responses are greatly reduced in animals with genetically-ablated AWC neurons[14] (Fig 1d, Supplementary Fig. 1d), suggesting a non-redundant role for AWC in the salt neural circuit. AWC neurons are glutamatergic and peptidergic[15], so we first investigated whether AWC signals the presence of high (+50 mM) salt to AIA by releasing glutamate. We knocked down the vesicular glutamate transporter, *eat-4*, which is essential for functional glutamatergic neurotransmission[16], specifically in AWC neurons. AWC-specific *eat-4* knockdown has no effect on AIA responses to +50 mM NaCl suggesting that glutamate was not the neurotransmitter (Fig. 1d). We then tested whether AWC signaling to AIA uses neuropeptides. Calcium-dependent secretion activator (CADPS) is an essential component of the release machinery for neuropeptide-containing dense core vesicles (*unc-31* in *C. elegans*)[17]. AWC-specific *unc-31* knockdown or ablating AWC significantly reduces AIA responses to +50 mM NaCl (Fig. 1d). This suggests that peptidergic signaling from AWC is a critical component of the high salt circuit. Neither AWC ablation nor knockdown of AWC peptide release machinery has an effect on AIA responses to +10 mM NaCl (within the 10 s post-stimulus addition period), as predicted from the unresponsiveness of AWC to this weak stimulus (Fig. 1e, Supplementary Fig. 1e). Our results reveal that AWC has different effects on AIA activity based on sensory modality. Previous work showed that, in an odor circuit, AWC-released glutamate inhibits AIA responses[15], while we show that, in the high salt circuit, AWC-released neuropeptides excite AIA.

To validate the salt circuit configurations characterized by imaging, we performed chemotaxis behavior assays to test whether AWC contributes to salt-driven behavior. In a salt chemotaxis assay, animals migrate towards a point source of NaCl over an hour[18] (Supplementary Fig. 3b). This behavior requires ASE neurons since *che-1* mutants which lack functional ASE neurons do not chemotax to salt[19] (Fig. 1f, n = 10 for all concentrations). Notably, AWC ablation causes a specific reduction in chemotaxis to steep, high salt gradients (with point sources of 500 and 750 mM NaCl, n = 10 and 10 respectively; “WT” n = 13 and 12 respectively), but has no effect on shallow, low salt gradient behavior (100 and 250 mM NaCl sources, n = 10 and 11; “WT” n = 10 and 10 respectively) (Fig. 1f). In fact, both the AWC^{ON} and AWC^{OFF} neurons contribute non-redundantly to high salt chemotaxis behavior (Supplementary Fig. 3c). Furthermore, *unc-31*-dependent neuropeptide release from AWC is necessary for chemotaxis to high salt sources, but dispensable for low salt-directed behavior (Fig. 1g, h). These results suggest that AWC signaling may increase the dynamic range of the salt circuit and prevent behavioral responses from saturating at high salt levels. The specific contribution of AWC neurons to high salt concentration behavior supports our imaging findings that AWC specifically responds to high, but not low salt stimuli (Fig. 1b, c).

AWC^{ON} acts as an interneuron in the salt circuit

The results described above suggest a crucial role for AWC neurons in the salt neural circuit and in salt-evoked behaviors. AWC^{ON} could adopt these roles either by intrinsically sensing salt, much like ASE[7], or by acting as an interneuron in an ASE-driven circuit. To distinguish between these two circuit configurations, we performed genetic manipulations that eliminate the ability of sensory neuron dendrites to contact the environment. We analyzed hypomorphic *osm-6* mutants that lack functional sensory cilia (dendritic endings) and found them to have greatly reduced ASEL salt responses and AWC^{ON} salt and odor responses[20] (Fig. 2b, c, Supplementary Fig. 4b, c). OSM-6 acts cell-autonomously[20]; therefore, we restored OSM-6 function under an ASEL cell-selective promoter and verified by confocal imaging that this enabled only ASEL, and not AWC^{ON}, to contact the environment (Fig. 2a, Supplementary Fig. 4a). In this ASEL-specific *osm-6* rescued animal, AWC^{ON} responds to +50 mM salt, suggesting that ASEL with functional cilia is sufficient to restore salt responses to AWC^{ON} (Fig. 2b, c Supplementary Fig. 4a, c). In contrast, rescuing *osm-6* under an AWC-selective promoter does not restore AWC^{ON} responses to salt, implying that AWC^{ON} alone is insufficient to respond to salt (Fig. 2b, Supplementary Fig. 4c). We confirmed that this rescuing array was functional as it fully restored the expected AWC^{ON} responses to the odor benzaldehyde (Fig. 2c). Taken together, these results indicate that AWC^{ON} is not an intrinsic salt sensor. Moreover, in the context of the high salt circuit, AWC acts as an interneuron by responding to a signal from ASEL.

Our work shows that ASEL to AWC^{ON} signaling functions in the adult. However, it is also possible that signaling between ASEL and AWC^{ON} may occur during development to instruct the wiring of the salt circuit. To probe this temporal requirement and eliminate the possibility of developmental contributions to the phenotypes observed in genetic mutants, we photo-ablated the ASEL neuron in the L4 larvae[21], and subsequently analyzed those adults. Consistently, AWC^{ON} neurons fail to respond to +50 mM NaCl after larval ASEL ablation, while mock ablation has no effect on salt responses (Fig. 2d). These results suggest that the observed ASEL-AWC^{ON} high salt circuit configuration is required in the adult and is not a consequence of changes in circuitry during early development.

AWC^{ON} salt responses require neuropeptides from ASEL

The results described above suggest that ASEL sensory neurons signal the presence of large increases in NaCl in the environment to the AWC^{ON} neurons, recruiting AWC^{ON} into the salt circuit. To further confirm the role of ASEL in mediating AWC^{ON} responses to salt, we tested the effects of manipulating ASEL neurotransmission. Mutations in *tom-1*, the *C. elegans* homolog of *Tomosyn*, which encodes a syntaxin interacting protein, upregulate all forms of neurotransmission[22] (for clarifying schematic see Supplementary Fig. 3a). We generated an ASEL-selective knockdown of *tom-1* to increase ASEL neurotransmitter and neuropeptide release. We hypothesized that enhanced transmission from ASEL would promote AWC^{ON} responses to the previously unresponsive +10 mM NaCl change. We found that AWC^{ON} did indeed respond to this small +10 mM stimulus in the ASEL-specific *tom-1* knockdown animal (Fig. 3a), confirming the crucial role of ASEL neurotransmission in initiating AWC^{ON} responses to salt.

C. elegans neurons including ASEL release amino acid and small molecule neurotransmitters, like glutamate, GABA and acetylcholine, from small, clear synaptic vesicles and neuropeptides from large, dense core vesicles[17]. We tested genetic mutants to identify the nature of the ASEL to AWC^{ON} signal. First, we analyzed mutants in *unc-13*, the *C. elegans* homolog of Munc13, which promotes the open syntaxin conformation needed for the release of small, clear synaptic vesicles[23] (Supplementary Fig. 3a). Surprisingly, we found that AWC^{ON} neurons continue to respond to +50 mM salt even in the *unc-13* mutants (Fig. 3b), suggesting that ASEL-AWC^{ON} communication does not require glutamate or other small molecule neurotransmitters. Therefore, we tested the salt responses of animals with a null mutation in the *C. elegans* homolog of Calcium-dependent secretion activator, *unc-31*, in which the release of dense core vesicles containing neuropeptides is defective[24] (Supplementary Fig. 3a). We found that AWC^{ON} responses to 50 mM increases in salt are eliminated in *unc-31* mutants and this gene is specifically required in ASEL (Fig. 3c). In contrast AWC^{OFF} neurons respond normally to +50 mM NaCl in both *unc-13* and *unc-31* mutants, suggesting that this neuron is an intrinsic sensor of large changes in salt (Supplementary Fig. 5a). Consistent with previous results, ASEL responses to salt are unchanged in *unc-13* and *unc-31* mutants[7] (Supplementary Fig. 5d). Taken together, these results suggest that ASEL detects large increases in salt and releases a neuropeptide to recruit AWC^{ON} into the salt circuit.

The *C. elegans* genome includes at least 113 neuropeptide genes (40 insulin-like, 31 FMRFamide-related and 42 other neuropeptide-like) that encode approximately 250 distinct neuropeptides[25]. In order to identify the cognate neuropeptide family, we tested mutants in the neuropeptide-processing pathway. Neuropeptides are synthesized as much larger propeptides, then cleaved by specific proprotein convertase enzymes and further modified to generate mature peptides. Four distinct proprotein convertases have been identified in the worm[25]. We hypothesized that in one or more proprotein convertase mutant, ASEL would not be able to process, cleave and release the mature peptide(s) necessary for recruiting AWC^{ON} to respond to high salt. Surprisingly, null mutations in *egl-3*, the major neuronal processor of FMRFamide-related peptides and neuropeptide-like proteins[26], as well as mutations in the convertases *kpc-1* and *aex-5*, do not alter AWC^{ON} responses to salt (Fig. 3d, Supplementary Fig. 5b). By contrast, a hypomorphic mutation in the proprotein convertase *bli-4*, which cleaves procollagens in the worm cuticle, but has no known function in the nervous system[27], blocks AWC^{ON} responses to salt (Fig. 3d). Furthermore, BLI-4 is specifically required in ASEL for AWC^{ON} salt responses (Fig. 3d, see also Supplementary Fig. 5b). We also tested ASEL responses to salt in *bli-4* mutants and found them to be normal (Supplementary Fig. 5e). These results suggest that ASEL uses a BLI-4 protease cleavage step downstream of salt detection to generate the mature peptide(s) that recruit AWC^{ON} into the salt circuit.

We confirmed a behavioral role for BLI-4 and ASEL-released neuropeptides using a salt chemotaxis assay. We found that animals with AWC-ablated, ASEL-specific knockdown of *unc-31*-dependent neuropeptide release, or ASEL-specific knockdown of *bli-4* (but not mutations in *egl-3*) show specific defects in attraction to a high concentration of salt (750 mM point source, Fig. 3e, Supplementary Fig. 3e), but have no effect on attraction to lower

salt (250 mM point source, Supplementary Fig. 3d). Taken together, these results indicate that ASEL uses BLI-4 cleavage to generate and release neuropeptides that modify the salt neural circuit and salt attraction behavior.

ASEL-released INS-6 recruits AWC^{ON} to the salt circuit

Mass spectrometry experiments show that the proprotein convertase EGL-3 processes many FMRFamide-like peptides and neuropeptide-like proteins, while BLI-4 has no role in processing these peptides[26]. We hypothesized that BLI-4 might instead cleave the remaining major class of neuropeptides (insulins), which are not detectable in these mass spectrometry studies[26]. Given that ASEL requires BLI-4 to communicate with AWC^{ON}, we analyzed the gene sequences of the 40 insulin-like peptides[25] and identified numerous genes containing the predicted BLI-4 cleavage sites[28] (Supplementary Table 2). We then imaged AWC^{ON} responses to high salt in animals with mutations in these candidate insulins. AWC^{ON} neurons in *ins-6* null mutants have significantly reduced responses to +50 mM NaCl (Fig. 4a). Normal responses are restored when *ins-6* is rescued specifically in ASEL (Fig. 4a, see also Supplementary Fig. 5c). Importantly, ASEL-specific expression of a mutated *ins-6* gene, in which two serine residues replace the two critical arginine amino acids in the predicted BLI-4 cleavage motif (RARR to RASS)[27], fails to rescue the mutant AWC^{ON} responses to salt (Fig. 4a). We also tested ASEL responses to salt in *ins-6* mutants and found them to be normal (Supplementary Fig. 5d). These data suggest that BLI-4 is required for the proteolytic processing that generates mature INS-6 peptides in ASEL, which signal to AWC^{ON}. However, the small, residual AWC^{ON} responses to high salt observed in *ins-6* mutants (Fig. 4a) suggest that there are additional neuropeptides relaying information from ASEL to AWC^{ON} neurons.

We hypothesized that INS-6 is also required for behavioral attraction to high concentrations of salt. In a chemotaxis assay, we found that *ins-6* mutants have a significant deficit in attraction to high salt (750 mM, Fig. 4b). ASEL-specific expression of the *ins-6* gene rescues this behavioral deficit; however, the mutant form of *ins-6*, in which the BLI-4 cleavage motif is disrupted, does not rescue the behavioral defect (Fig. 4b, Supplementary Fig. 3e). Furthermore, we found that these mutants behave normally in low salt gradients (Supplementary Fig. 3f). Together, these results suggest a novel role for BLI-4 cleavage in the production of a mature insulin-like peptide, INS-6, which recruits AWC^{ON} neurons to the high salt neural circuit and specifically potentiates attraction to high salt.

DAF-2/AGE-1 pathway acts in AWC^{ON} in the high salt circuit

Previous studies showed that INS-6 binds the human insulin receptor and functions as an agonist[29]. Therefore, to identify the *C. elegans* INS-6 receptor and the downstream signaling machinery that might function in AWC^{ON}, we probed the canonical insulin-signaling cascade. We analyzed animals with hypomorphic mutations in the *C. elegans* homolog of the mammalian insulin/IGF receptor tyrosine kinase, *daf-2*[30]. We found that AWC^{ON} responses to +50 mM salt are greatly attenuated in *daf-2* mutants (Fig. 4c). Moreover, restoring function of this receptor to AWC specifically is sufficient to restore normal AWC^{ON} responses to salt (Fig. 4c). We then tested partial loss of function mutants of *age-1*, the *C. elegans* PI3-Kinase homolog, which has been shown to act downstream of the DAF-2

insulin receptor[31]. AWC^{ON} NaCl responses are much reduced in *age-1* mutants and normal responses are restored to animals when AGE-1 function is specifically rescued in AWC^{ON} (Fig. 4d). ASEL responses to salt are not affected in *daf-2* or *age-1* mutants, suggesting that insulin signaling functions downstream of the stimulus detection (Supplementary Fig. 5e). These results indicate that AWC^{ON} neurons may use DAF-2 and AGE-1 to detect the ASEL-released insulin-like peptides and to signal the presence of large changes in salt to the downstream circuit.

In addition, we performed epistasis experiments to determine the genetic relationship between these canonical insulin signaling pathway components and the ASEL neuropeptide processing and release machinery. We found that the endoprotease BLI-4 acts upstream of the DAF-2 insulin receptor and AGE-1. Knocking down *bli-4* in ASEL completely blocks DAF-2- and AGE-1-dependent AWC^{ON} responses to salt. (Fig. 4e, compared to Fig. 4c, d). We also tested whether the weak AWC^{ON} responses to +10 mM NaCl observed in the *tom-1* knockdown (shown in Fig. 3a) were regulated by the same insulin signaling pathway. Consistently, we found that these AWC^{ON} responses are lost in the *ins-6*, *daf-2* or *age-1* mutants (Fig. 4f). This suggests that an effect of ASEL-specific *tom-1* knockdown may be to increase INS-6 release, and this peptide is necessary for the weak AWC^{ON} responses to +10 mM NaCl. Additionally, these results indicate that neuropeptide processing in ASEL and transmitter release from ASEL function upstream of the insulin receptor and PI3-Kinase in the pathway that recruits AWC^{ON} to the high salt circuit.

DISCUSSION

Our results show that *C. elegans* chemosensory neural circuits are flexible and their neuronal composition can be modified by sensory context and insulin neuropeptide signals. Previous studies and our results show that ASEL responds to an increase in NaCl in the environment[7]. Notably, we show that the circuit downstream of ASEL exists in two different configurations: at small changes in NaCl (< 20 mM), we find that ASEL neurons signal directly to downstream, classically-defined interneurons (Supplementary Fig. 6a). However, at larger changes in NaCl (> 20 mM), ASEL neurons release INS-6 and other neuropeptides to functionally transform the AWC^{ON} sensory neuron into an interneuron and recruit it into the salt circuit (Supplementary Fig. 6b). These results show that sensory context and peptide signals switch the response profile of AWC^{ON} neurons and modulate the information that is relayed to downstream circuitry. Consistent with these results, AWC plays a crucial role in transmitting information to the downstream AIA interneurons and in mediating salt behaviors. Our behavioral analyses indicate that this novel ASEL–AWC^{ON} neuropeptide signaling is likely to potentiate attraction to high, but not low concentrations of salt. The unique insulin-regulated high salt circuit configuration may be critical in reinforcing salt appetite, perhaps to maintain ion homeostasis that is needed for organ system functioning[33]. Similarly, investigations of mammalian salt circuits show that distinct sets of taste sensory neurons detect high and low salt, with particular neuronal populations contributing to appetitive behaviors[9].

Insulin signaling is highly conserved between mammals and *C. elegans*, with well-characterized roles in the regulation of food intake, glucose metabolism and aging[34, 35]. In

the mammalian brain, insulin signals modulate the firing of hypothalamic neurons[36] and olfactory sensory neurons[37]. In *C. elegans*, neuronal insulin signaling regulates chemotaxis[38], thermotaxis[39] and learning[40]. However, less is known about the relevant machinery for processing and releasing insulins. Our results demonstrate that insulin signals may be released from dense core vesicles in a Calcium-dependent secretion activator (UNC-31)-dependent manner, and this action remodels sensory circuits. Furthermore, our data suggests that the insulin-like peptide, INS-6, is processed at a dibasic motif by a proprotein convertase, BLI-4. Insulin-like peptides may in fact be cleaved through diverse mechanisms at different developmental stages and in different cell types. A recent study showed that pan-neuronally expressed INS-6 can be processed by the proprotein convertase EGL-3[41]. In this instance, the mature INS-6 peptide functions as a long-range signal to instruct the development of the neuromuscular junction[41]. In contrast, our results show that BLI-4 in ASEL generates mature INS-6 peptides that act locally to rapidly recruit AWC^{ON} into the adult salt circuit. Additionally, INS-6 released from ASI neurons has been shown to influence the transcription of another insulin (INS-7) and modify aversive olfactory learning[42]. These results show that the protein processing machinery regulates the activity of mature peptides both spatially and temporally to modulate both the developing and adult nervous systems. Moreover, these multi-functional roles of INS-6 in development and circuit plasticity are consistent with previous studies showing distinct roles for the same insulin ligand[15, 38].

Our epistasis experiments demonstrate that BLI-4-dependent insulin processing in ASEL occurs upstream of the insulin peptides binding to the insulin receptor tyrosine kinase, DAF-2, and signaling via the PI3-Kinase, AGE-1 (Supplementary Fig. 6b). Salt-evoked calcium responses in AWC^{ON} occur downstream of PI3-Kinase activation suggesting a link between intracellular signaling and AWC^{ON} neuronal activation. Moreover, our results suggest that ASEL neurons may release other insulin-like peptides along with INS-6 that likely also signal through this canonical insulin pathway to activate AWC^{ON}.

There is increasing evidence in a number of species that sensory signaling is modulated by neuromodulators and external milieu. In *Drosophila*, variable levels of metabotropic $GABA_B$ receptor expression expand the dynamic range of the olfactory system to drive flexible and ecologically appropriate behavioral outputs[43]. Non-synaptic, lateral signaling between olfactory receptor neurons also modifies the sensory information relayed to the downstream circuit in certain complex olfactory contexts[44]. However, the underlying molecular machinery is largely unknown. Collectively, these studies and ours provide additional detail about how neuropeptides and other modulatory signals fine-tune sensory encoding to generate flexible behaviors.

We show that sensory context (in our case the concentration of salt) causes a rapid switch in the neural circuit and a novel ASEL-AWC^{ON} insulin neuropeptide signaling cascade mediates this switch. Neuropeptides have been previously shown to play crucial roles in switching neural circuits, particularly in the stomatogastric ganglion of the crab[45]. Neuromodulators can switch individual neurons, such as VD motor neurons, from a sub-circuit that drives a fast pyloric rhythm to a slower gastric rhythm circuit and vice versa[46,47]. Interestingly, sensory context can also drive a switch in the vertebrate retinal circuitry. At

low light levels, inputs from cone and rod photoreceptors converge onto cone bipolar cells. However, as light intensity increases or in presence of neuromodulators like dopamine and nitric oxide, inputs from rod photoreceptors are turned off. Uncoupling the amacrine AII cells prevents rod cell signals from being relayed to cone bipolar cells to accomplish this circuit modification[3, 48]. Nevertheless, the precise mechanisms for releasing and detecting the modulatory cues that switch these crustacean and mammalian circuits remain to be elucidated. Therefore, while there is precedence for neuropeptides remodeling neural networks, we find that the ASEL-AWC^{ON}-AIA circuit is unique in its context-dependent and insulin-mediated functional transformation of the AWC^{ON} sensory neuron into an interneuron.

Finally, our results suggest that neural circuits are highly flexible and neuroanatomy is only an important first step towards analyzing brain function. The complete *C. elegans* wiring diagram was mapped from electron microscope reconstructions[4]. However, this information is not sufficient to explain the intricate functioning of neural circuits in complex environments. We suggest one explanation for this discrepancy: information can be relayed through numerous alternative neural paths, including flowing through sensory neurons that transiently act like interneurons, depending on environmental context and modulatory states. We speculate that the highly interconnected nature of vertebrate brains[49] represents alternate paths for information processing and propose that neuropeptide signaling selects active routes based on context. These flexible neural circuit configurations may be critical for responding to novel and dynamic sensory environments.

METHODS

C. elegans strains (Supplementary Table 1) were grown and maintained under standard conditions, at 20 degrees C[50].

Molecular biology and transgenesis

cDNA corresponding to the entire coding sequences of *osm-6*, *tom-1*, *unc-31*, *eat-4*, *daf-2*, and *age-1* was amplified by PCR and expressed under cell-selective promoters. *ins-6* genomic DNA was amplified by PCR and two point mutations (AC to TA) were generated to change the basic arginine residues in the predicted BLI-4 cleavage site[27] to serines (using the Agilent QuikChange II Site-Directed Mutagenesis Kit, primers 5′–CAATGCCACGAGCAAG**TA**GTGTTCCAGCACCAG and 5′–CTGGTGCTGGAACAC**TA**CTTGCTCGTGGCATTG). Neuron-selective RNAi transgenes were created as previously described by co-injection of equal concentrations of sense and antisense oriented gene fragments driven by cell-specific promoters[51]. For *bli-4* knockdowns, a fragment matching exons 2–10, containing the protease domain, was synthesized (GenScript) and subcloned in both orientations. For light-inducible ASEL cell ablations and mock ablations, miniSOG was targeted to the mitochondrial outer membrane (tomm-20(N’55AA)::miniSOG) and expressed under an ASEL cell-specific promoter[21]. Cell-specific expression was achieved using the following promoters: *gcy-7* for ASEL, *gcy-5* for ASER, *odr-3* or *ceh-36* for AWC, *str-2* for AWC^{ON}, *srsx-3* for AWC^{OFF}, *ins-1* for AIA, *gpa-4* for AWA and ASI, *str-3* for ASI, *str-1* for AWB, *sra-6* for ASH and *sra-9* for

ASK. For all experiments, a splice leader (SL2) fused to a *mCherry* transgene was used to confirm cell-specific expression of the gene of interest.

Germline transformations were performed by microinjection of plasmids at concentrations between 25 and 100 ng/μl with 10 ng/μl of *unc-122::rfp*, *unc-122::gfp* or *elt-2::gfp* as a co-injection marker. For rescue experiments, DNA was injected into mutant *C. elegans* carrying GCaMP arrays. For cell-specific RNAi knockdown experiments, sense and antisense DNA was injected into wild-type or mutant worms.

Calcium imaging

Transgenic worms with GCaMP expressed under a cell-specific promoter were trapped in a custom designed PDMS microfluidic device[52] and exposed to salt stimuli. Fluorescence from the neuronal cell body was captured using a Zeiss inverted compound microscope for 3 minutes. We first captured 10 s of baseline activity in chemotaxis assay buffer (5 mM potassium phosphate (pH 6), 1 mM $CaCl_2$, 1 mM $MgSO_4$, and 50 mM NaCl), then 2 min of exposure to a higher NaCl concentration chemotaxis buffer stimulus, and lastly 50 s of buffer only.

We used Metamorph and an EMCCD camera (Photometrics) to capture images at a rate of 10 frames per s. For all sensory neurons, the average fluorescence in a 3 s window (t = 1–4 s) was set as F_0. For the AIA interneuron imaging, baseline fluorescence was more variable; therefore, a 10 s window (t = 0–10 s) was set as F_0. A Matlab script was used to analyze the average fluorescence for the cell body region of interest and to plot the percent change in fluorescence for the region of interest relative to F_0, as previously described[32]. For all figures, average and standard errors at each time point were generated and plotted in Matlab. For statistical analysis, the average fluorescence and standard error were calculated for each animal over the 10 s period following the addition of the salt stimulus (t = 10–20 s). For the bar graph in the benzaldehyde odor experiment (Fig. 2c), the average fluorescence and standard error were calculated over the 10 s period after odor removal (t = 130–140 s), with the 3 s window from t = 121–124 s set as F_0. Two-tailed unpaired *t*-tests were used to compare the responses of different genotypes, and the Bonferroni correction was used to adjust for multiple comparisons. No statistical methods were used to pre-determine sample sizes; however, our sample sizes are similar to those reported in previous publications[7, 32]. Data distribution was assumed to be normal, but this was not formally tested. Wild-type controls, mutants, and rescue strains for each figure were imaged in alternation, in the same session. A single neuron was imaged in each animal, and each animal was imaged only once. No data points were excluded. Data collection and analysis were not performed blind to the conditions of the experiments.

Chemotaxis assays

Chemotaxis assays to sodium chloride were performed as previously described[18]. Assays were performed on 2% agar plates (10 cm) containing 5 mM potassium phosphate (pH 6), 1 mM $CaCl_2$ and 1 mM $MgSO_4$. Concentration gradients of NaCl were established by placing a 5 mm agar plug from a 100, 250, 500 or 750 mM NaCl agar plate near the edge of the plate and a control 0 mM NaCl agar plug at the opposite end of the plate. Plugs were

removed after 18–20 hours and 1 μl of 1 M sodium azide solution was spotted in the locations previously occupied by the plugs. Animals were washed once in M9 and three times in chemotaxis buffer (5 mM potassium phosphate (pH 6), 1 mM $CaCl_2$ and 1 mM $MgSO_4$). Worms were placed on the plate and allowed to move freely for one hour. The chemotaxis index was computed as the number of worms in the region near the high salt minus the worms in the region near the control divided by the total number of worms that moved beyond the origin. Experiments were performed over 4 or more days; average chemotaxis indices of 9–15 assay plates are presented. Our sample sizes are similar to those reported in previous publications[8, 18, 32, 38]. Data distribution was assumed to be normal, but this was not formally tested. Two-tailed unpaired *t*-tests were used to compare the responses of different genotypes, and the Bonferroni correction was used to adjust for multiple comparisons. Data collection and analysis were not performed blind to the conditions of the experiments.

Confocal cilia imaging

Anesthetized young adult worms were imaged on a 2% agarose pad. Images were captured on a Zeiss LSM780 confocal microscope using a 40X objective and maximum intensity projections were generated using Zeiss Zen software. Dendritic cilia were imaged in 4–7 individual animals of each genotype, and the cilia morphology was found to be nearly identical in all animals of the same condition.

miniSOG light-inducible cell ablation

ASEL neurons were ablated or mock ablated in larval (L4) stage transgenic worms with miniSOG specifically targeted to the outer mitochondrial membrane of ASEL. Ablation was performed, using a Zeiss inverted compound microscope equipped with an X-Cite 120Q series fluorescence illumination lamp with the objective removed, by exposing freely moving animals to 90 minutes of pulsed (0.5 s on, 1.5 s off) 488 nm, blue light, as previously described[21]. Animals appeared to move normally and remain healthy after this illumination. Successful neuronal ablation was confirmed by the absence of ASEL mCherry fluorescence 16 to 24 hours later (prior to calcium imaging). A different wavelength (510 nm, green) light was similarly pulsed for mock ablation experiments[21] and it was confirmed that this did not alter ASEL mCherry fluorescence.

Supplementary Material

Refer to Web version on PubMed Central for supplementary material.

Acknowledgments

We thank the *Caenorhabditis* Genetics Center, the National Brain Research Project, Japan, C. Bargmann, P. Sengupta, P. Sternberg and A. Zaslaver for strains, M. Ailion for *unc-31* cDNA, Y. Jin, C. Stevens, T. Sejnowski, E.J. Chichilnisky and H. Karten for helpful discussions. We also acknowledge J. Fitzpatrick and J. Kasuboski of the Waitt Advanced Biophotonics Center for providing the resources and training to perform confocal imaging and J. Simon for help with the illustrations. And, we are grateful to A. Tong, C. Yang and other members of the Chalasani laboratory for critical help, advice and insights. This work was funded by grants from The Searle Scholars Program, March of Dimes, Whitehall Foundation, Rita Allen Foundation and the NIH R01MH096881-01A1 (S.H.C.). S.G.L. holds a graduate research fellowship from the NSF.

References

1. Touhara K, Vosshall LB. Sensing odorants and pheromones with chemosensory receptors. Annu Rev Physiol. 2009; 71:307–332. [PubMed: 19575682]
2. Weimann JM, Marder E. Switching neurons are integral members of multiple oscillatory networks. Curr Biol. 1994; 4:896–902. [PubMed: 7850423]
3. Baldridge WH, Vaney DI, Weiler R. The modulation of intercellular coupling in the retina. Semin Cell Dev Biol. 1998; 9:311–318. [PubMed: 9665867]
4. White JG, Southgate E, Thomson JN, Brenner S. The structure of the nervous system of the nematode *Caenorhabditis elegans*. Phil Transact R Soc Lond B. 1986; 314:1–340.
5. de Bono M, Maricq AV. Neuronal substrates of complex behaviors in C. elegans. Annu Rev Neurosci. 2005; 28:451–501. [PubMed: 16022603]
6. Bargmann CI, Horvitz HR. Chemosensory neurons with overlapping functions direct chemotaxis to multiple chemicals in C. elegans. Neuron. 1991; 7:729–742. [PubMed: 1660283]
7. Suzuki H, et al. Functional asymmetry in Caenorhabditis elegans taste neurons and its computational role in chemotaxis. Nature. 2008; 454:114–117. [PubMed: 18596810]
8. Wes PD, Bargmann CIC. elegans odour discrimination requires asymmetric diversity in olfactory neurons. Nature. 2001; 410:698–701. [PubMed: 11287957]
9. Chandrashekar J, et al. The cells and peripheral representation of sodium taste in mice. Nature. 2010; 464:297–301. [PubMed: 20107438]
10. Bargmann CI. Chemosensation in C. elegans. WormBook. 2006:1–29. [PubMed: 18050433]
11. Ramot D, MacInnis BL, Goodman MB. Bidirectional temperature-sensing by a single thermosensory neuron in C. elegans. Nat Neurosci. 2008; 11:908–915. [PubMed: 18660808]
12. Clark DA, Biron D, Sengupta P, Samuel AD. The AFD sensory neurons encode multiple functions underlying thermotactic behavior in Caenorhabditis elegans. J Neurosci. 2006; 26:7444–7451. [PubMed: 16837592]
13. Thiele TR, Faumont S, Lockery SR. The neural network for chemotaxis to tastants in Caenorhabditis elegans is specialized for temporal differentiation. J Neurosci. 2009; 29:11904–11911. [PubMed: 19776276]
14. Beverly M, Anbil S, Sengupta P. Degeneracy and neuromodulation among thermosensory neurons contribute to robust thermosensory behaviors in Caenorhabditis elegans. J Neurosci. 2011; 31:11718–11727. [PubMed: 21832201]
15. Chalasani SH, et al. Neuropeptide feedback modifies odor-evoked dynamics in Caenorhabditis elegans olfactory neurons. Nat Neurosci. 2010; 13:615–621. [PubMed: 20364145]
16. Lee RY, Sawin ER, Chalfie M, Horvitz HR, Avery L. EAT-4, a homolog of a mammalian sodium-dependent inorganic phosphate cotransporter, is necessary for glutamatergic neurotransmission in caenorhabditis elegans. J Neurosci. 1999; 19:159–167. [PubMed: 9870947]
17. Richmond J. Synaptic function. WormBook. 2005:1–14. [PubMed: 18050398]
18. Ward S. Chemotaxis by the nematode Caenorhabditis elegans: identification of attractants and analysis of the response by use of mutants. Proc Natl Acad Sci U S A. 1973; 70:817–821. [PubMed: 4351805]
19. Uchida O, Nakano H, Koga M, Ohshima Y. The C. elegans che-1 gene encodes a zinc finger transcription factor required for specification of the ASE chemosensory neurons. Development. 2003; 130:1215–1224. [PubMed: 12588839]
20. Collet J, Spike CA, Lundquist EA, Shaw JE, Herman RK. Analysis of osm-6, a gene that affects sensory cilium structure and sensory neuron function in Caenorhabditis elegans. Genetics. 1998; 148:187–200. [PubMed: 9475731]
21. Qi YB, Garren EJ, Shu X, Tsien RY, Jin Y. Photo-inducible cell ablation in Caenorhabditis elegans using the genetically encoded singlet oxygen generating protein miniSOG. Proc Natl Acad Sci U S A. 2012; 109:7499–7504. [PubMed: 22532663]
22. Gracheva EO, et al. Tomosyn negatively regulates both synaptic transmitter and neuropeptide release at the C. elegans neuromuscular junction. J Physiol. 2007; 585:705–709. [PubMed: 17627987]

23. Richmond JE, Davis WS, Jorgensen EM. UNC-13 is required for synaptic vesicle fusion in C. elegans. Nat Neurosci. 1999; 2:959–964. [PubMed: 10526333]
24. Speese S, et al. UNC-31 (CAPS) is required for dense-core vesicle but not synaptic vesicle exocytosis in Caenorhabditis elegans. J Neurosci. 2007; 27:6150–6162. [PubMed: 17553987]
25. Li C, Kim K. Neuropeptides. WormBook. 2008:1–36. [PubMed: 18819171]
26. Husson SJ, Clynen E, Baggerman G, Janssen T, Schoofs L. Defective processing of neuropeptide precursors in Caenorhabditis elegans lacking proprotein convertase 2 (KPC-2/EGL-3): mutant analysis by mass spectrometry. J Neurochem. 2006; 98:1999–2012. [PubMed: 16945111]
27. Thacker C, Peters K, Srayko M, Rose AM. The bli-4 locus of Caenorhabditis elegans encodes structurally distinct kex2/subtilisin-like endoproteases essential for early development and adult morphology. Genes Dev. 1995; 9:956–971. [PubMed: 7774813]
28. Thacker C, Sheps JA, Rose AM. Caenorhabditis elegans dpy-5 is a cuticle procollagen processed by a proprotein convertase. Cell Mol Life Sci. 2006; 63:1193–1204. [PubMed: 16649143]
29. Hua QX, et al. A divergent INS protein in Caenorhabditis elegans structurally resembles human insulin and activates the human insulin receptor. Genes Dev. 2003; 17:826–831. [PubMed: 12654724]
30. Kimura KD, Tissenbaum HA, Liu Y, Ruvkun G. daf-2, an insulin receptor-like gene that regulates longevity and diapause in Caenorhabditis elegans. Science. 1997; 277:942–946. [PubMed: 9252323]
31. Dorman JB, Albinder B, Shroyer T, Kenyon C. The age-1 and daf-2 genes function in a common pathway to control the lifespan of Caenorhabditis elegans. Genetics. 1995; 141:1399–1406. [PubMed: 8601482]
32. Chalasani SH, et al. Dissecting a circuit for olfactory behaviour in Caenorhabditis elegans. Nature. 2007; 450:63–70. [PubMed: 17972877]
33. Aburto NJ, et al. Effect of lower sodium intake on health: systematic review and meta-analyses. BMJ. 2013; 346:f1326. [PubMed: 23558163]
34. Tissenbaum HA. Genetics, life span, health span, and the aging process in Caenorhabditis elegans. J Gerontol A Biol Sci Med Sci. 2012; 67:503–510. [PubMed: 22499764]
35. Taguchi A, White MF. Insulin-like signaling, nutrient homeostasis, and life span. Annu Rev Physiol. 2008; 70:191–212. [PubMed: 17988211]
36. Klockener T, et al. High-fat feeding promotes obesity via insulin receptor/PI3K-dependent inhibition of SF-1 VMH neurons. Nat Neurosci. 2011; 14:911–918. [PubMed: 21642975]
37. Savigner A, et al. Modulation of spontaneous and odorant-evoked activity of rat olfactory sensory neurons by two anorectic peptides, insulin and leptin. J Neurophysiol. 2009; 101:2898–2906. [PubMed: 19297511]
38. Tomioka M, et al. The insulin/PI 3-kinase pathway regulates salt chemotaxis learning in Caenorhabditis elegans. Neuron. 2006; 51:613–625. [PubMed: 16950159]
39. Murakami H, Bessinger K, Hellmann J, Murakami S. Aging-dependent and -independent modulation of associative learning behavior by insulin/insulin-like growth factor-1 signal in Caenorhabditis elegans. J Neurosci. 2005; 25:10894–10904. [PubMed: 16306402]
40. Kauffman AL, Ashraf JM, Corces-Zimmerman MR, Landis JN, Murphy CT. Insulin signaling and dietary restriction differentially influence the decline of learning and memory with age. PLoS Biol. 2010; 8:e1000372. [PubMed: 20502519]
41. Hung WL, et al. Attenuation of insulin signalling contributes to FSN-1-mediated regulation of synapse development. Embo J. 2013
42. Chen Z, et al. Two insulin-like peptides antagonistically regulate aversive olfactory learning in C. elegans. Neuron. 2013; 77:572–585. [PubMed: 23395381]
43. Root CM, et al. A presynaptic gain control mechanism fine-tunes olfactory behavior. Neuron. 2008; 59:311–321. [PubMed: 18667158]
44. Su CY, Menuz K, Reisert J, Carlson JR. Non-synaptic inhibition between grouped neurons in an olfactory circuit. Nature. 2012; 492:66–71. [PubMed: 23172146]
45. Dickinson PS, Mecsas C, Marder E. Neuropeptide fusion of two motor-pattern generator circuits. Nature. 1990; 344:155–158. [PubMed: 2308633]

46. Weimann JM, Meyrand P, Marder E. Neurons that form multiple pattern generators: identification and multiple activity patterns of gastric/pyloric neurons in the crab stomatogastric system. J Neurophysiol. 1991; 65:111–122. [PubMed: 1999725]

47. Hooper SL, Moulins M. Switching of a neuron from one network to another by sensory-induced changes in membrane properties. Science. 1989; 244:1587–1589. [PubMed: 2740903]

48. Xia XB, Mills SL. Gap junctional regulatory mechanisms in the AII amacrine cell of the rabbit retina. Vis Neurosci. 2004; 21:791–805. [PubMed: 15683564]

49. Markov NT, et al. A Weighted and Directed Interareal Connectivity Matrix for Macaque Cerebral Cortex. Cereb Cortex. 2012

50. Brenner S. The genetics of Caenorhabditis elegans. Genetics. 1974; 77:71–94. [PubMed: 4366476]

51. Esposito G, Di Schiavi E, Bergamasco C, Bazzicalupo P. Efficient and cell specific knock-down of gene function in targeted C. elegans neurons. Gene. 2007; 395:170–176. [PubMed: 17459615]

52. Chronis N, Zimmer M, Bargmann CI. Microfluidics for in vivo imaging of neuronal and behavioral activity in Caenorhabditis elegans. Nat Methods. 2007; 4:727–731. [PubMed: 17704783]

53. Chen BL, Hall DH, Chklovskii DB. Wiring optimization can relate neuronal structure and function. Proc Natl Acad Sci U S A. 2006; 103:4723–4728. [PubMed: 16537428]

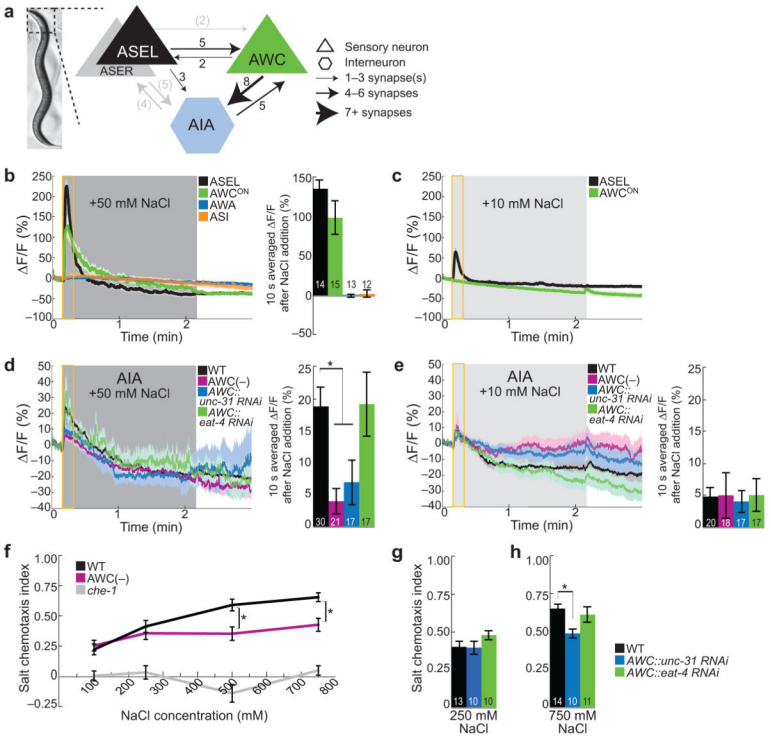

Figure 1. A distributed neural network encodes salt concentration

(**a**) Synapses and synaptic weights[53] between ASEL, ASER and AWC sensory neurons and onto AIA interneurons in the head of *C. elegans*. (**b**) Average GCaMP fluorescence change in wild-type sensory neurons in response to +50 mM NaCl. (**c**) Fluorescence change in wild-type ASEL (10 s averaged ΔF/F after salt addition is 31.74 ± 5.76 (s.e.m), n = 13) and AWC^{ON} (–6.97 ± 0.81, n = 13) sensory neurons in response to +10 mM NaCl. (**d, e**) AIA interneuron responses of wild-type, AWC-ablated, AWC-specific knockdown of *unc-31*(the *C. elegans* homolog of Calcium-dependent secretion activator) and AWC-specific knockdown of *eat-4* (the *C. elegans* vesicular glutamate transporter) worms to +50 mM NaCl (**d**) and +10 mM NaCl (**e**). *Significantly different from wild-type ($P < 0.05$, two-tailed *t*-test with Bonferroni correction). (**b–e**) Dark and light gray shading indicates 2 minute +50 mM or +10 mM NaCl stimulus, respectively, beginning at t = 10 s. Numbers on bars indicate number of neurons imaged. Yellow box indicates the 10 s after stimulus addition, for which the fluorescence change is averaged in the bar graphs. The light color shading around curves and the error bars on bar graphs indicate s.e.m. (**f**) Salt chemotaxis of wild-type, AWC-ablated, and *che-1* (no ASE) mutant worms to a range of salt concentrations. (**g, h**) Chemotaxis of wild-type, AWC-specific *unc-31* knockdown, and AWC-specific *eat-4* knockdown to a low 250 mM NaCl point source (**g**) or a high 750 mM NaCl point source (**h**). Numbers on bars indicate number of assay plates. (**f–h**) Error bars indicate s.e.m. *Significantly different from wild-type, as indicated ($P < 0.05$, two-tailed *t*-test with Bonferroni correction).

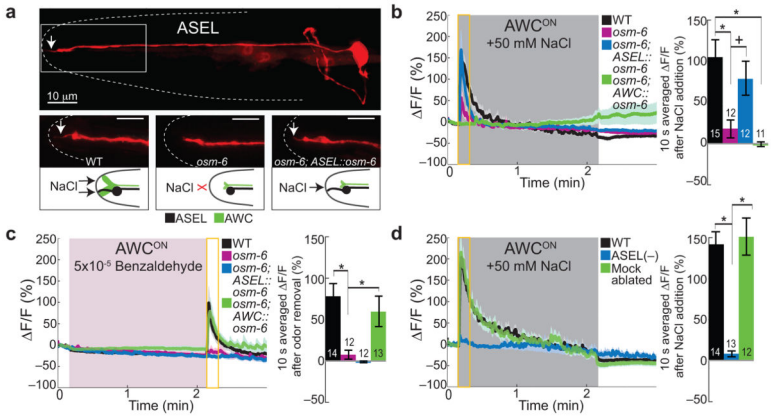

Figure 2. AWC^{ON} sensory neurons act as interneurons in the salt circuit

(**a**) Confocal images and diagrams of the ASEL neuron (i) and cilia morphology (ii–iv) in wild-type (i, ii), *osm-6* mutant (iii), and *osm-6; ASEL::osm-6* cell-specific rescue (iv). White arrow indicates elaborated cilia structure in wild-type and *osm-6*; ASEL::osm-6 cell-specific rescue. Scale bar 10 µm. (**b, c**) AWC^{ON} wild-type, *osm-6* mutant, *osm-6; ASEL::osm-6* and *osm-6; AWC::osm-6* responses to +50 mM NaCl (**b**) and a 5×10^{-5} dilution of benzaldehyde odor (**c**). (**d**) AWC^{ON} responses to +50 mM NaCl in wild-type and in transgenic worms in which ASEL neurons were photo-ablated or mock ablated in larvae. (**b–d**) Numbers on bars indicate number of neurons imaged. Yellow box indicates the 10 s time period for which the fluorescence change is averaged in the bar graphs. Light color shading around curves and bar graph error bars indicate s.e.m. *Significantly different from wild-type or mutant, as indicated ($P < 0.05$, two-tailed *t*-test with Bonferroni correction). +($P < 0.1$, two-tailed *t*-test with Bonferroni correction).

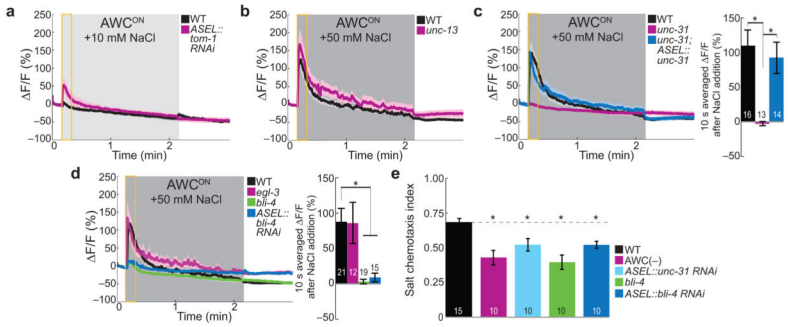

Figure 3. AWC^{ON} salt responses require peptidergic neurotransmission from ASEL

(**a**) AWC^{ON} average calcium responses to +10 mM NaCl in wild-type (averaged ΔF/F after salt addition is −6.15 ± 1.32, n = 21) and ASEL-specific *tom-1* (Tomosyn homolog) knockdown (32.13 ± 18.56, $P < 0.05$ compared to WT, n = 12). (**b**) AWC^{ON} responses to +50 mM NaCl in wild-type (94.26 ± 22.26, n = 15) and *unc-13* mutants (102.38 ± 30.70, n = 12). **(a, b)** Numbers in parentheses are mean ± s.e.m. (**c, d**) AWC^{ON} responses to +50 mM NaCl in *unc-31* mutants and *unc-31; ASEL::unc-31* cell-specific rescue (**c**), and *egl-3*, *bli-4*, and ASEL-specific *bli-4* knockdown (**d**). Numbers on bars indicate number of neurons imaged. *Significantly different from wild-type or mutant, as indicated ($P < 0.05$, two-tailed *t*-test with Bonferroni correction). (**a–d**) Light color shading around curves and bar graph error bars indicate s.e.m. (**e**) High salt (750 mM point source) chemotaxis of wild-type, AWC-ablated, ASEL-specific *unc-31 RNAi*, *bli-4*, and ASEL-specific *bli-4 RNAi* worms. Numbers on bars indicate number of assay plates. Error bars indicate s.e.m. *Significantly different from wild-type ($P < 0.05$, two-tailed *t*-test with Bonferroni correction).

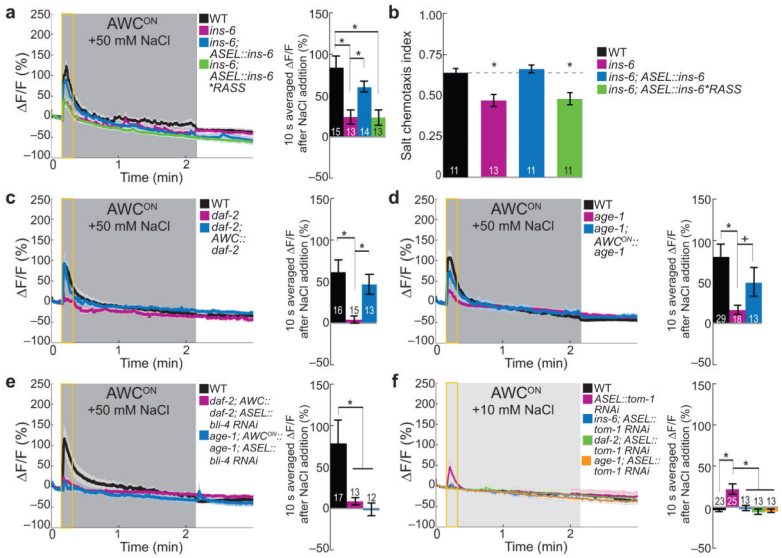

Figure 4. INS-6 signals through DAF-2 and AGE-1 to remodel the ASEL-AWC^{ON} salt circuit

(**a**) AWC^{ON} calcium responses to +50 mM NaCl in wild-type, insulin-like peptide *ins-6* mutants, and *ASEL::ins-6* rescue with or without mutations that replace the two critical arginine amino acids in the predicted BLI-4 cleavage motif with two serine residues (*RASS). (**b**) High salt (750 mM point source) chemotaxis of wild-type, *ins-6* mutant, *ASEL::ins-6* cell-specific rescue, and BLI-4 cleavage motif mutated *ASEL::ins-6*RASS* transgenic worms. Error bars indicate s.e.m. *Significantly different from wild-type ($P < 0.05$, *t*-test with Bonferroni correction). (**c, d**) Mutant AWC^{ON} responses to +50 mM NaCl. (**c**) Insulin-like receptor, *daf-2*, mutant and *AWC::daf-2* rescue. (**d**) PI3-Kinase, *age-1*, mutant and *AWC^{ON}::age-1* rescue. (**e**) AWC^{ON} responses to +50 mM NaCl in wild-type and in transgenic animals with ASEL-specific knockdown of the peptide processing enzyme *bli-4* in a *daf-2* mutant background with AWC-specific *daf-2* rescue or in an *age-1* background with AWC^{ON}-specific *age-1* rescue. (**f**) AWC^{ON} responses to +10 mM NaCl in wild-type and in ASEL-specific *tom-1* (*Tomosyn*) knockdown in a wild-type background or in an *ins-6*, *daf-2* or *age-1* mutant background. (**a, c–f**) Light color shading around curves and bar graph error bars indicate s.e.m. *Significantly different from wild-type or mutant, as indicated ($P < 0.05$, two-tailed *t*-test with Bonferroni correction). +($P < 0.1$, two-tailed *t*-test with Bonferroni correction).